Molecularly Targeted Radiosensitization of Human Prostate Cancer by Modulating Inhibitor of Apoptosis

Yao Dai,[1] Meilan Liu,[1] Wenhua Tang,[1] Jeffrey DeSano,[1] Ezra Burstein,[2] Mary Davis,[1] Kenneth Pienta,[2,3] Theodore Lawrence,[1] and Liang Xu[1]

Abstract

Purpose: The inhibitor of apoptosis proteins (IAP) are overexpressed in hormone-refractory prostate cancer, rendering the cancer cells resistant to radiation. This study aims to investigate the radiosensitizing effect of small-molecule IAP inhibitor both *in vitro* and *in vivo* in androgen-independent prostate cancer and the possible mechanism of radiosensitization.

Experimental Design: Radiosensitization of SH-130 in human prostate cancer DU-145 cells was determined by clonogenic survival assay. Combination effect of SH-130 and ionizing radiation was evaluated by apoptosis assays. Pull-down and immunoprecipitation assays were employed to investigate the interaction between SH-130 and IAPs. DU-145 xenografts in nude mice were treated with SH-130, radiation, or combination, and tumor suppression effect was determined by caliper measurement or bioluminescence imaging. Nuclear factor-κB activation was detected by luciferase reporter assay and quantitative real-time PCR.

Results: SH-130 potently enhanced radiation-induced caspase activation and apoptosis in DU-145 cells. Both X-linked IAP and cIAP-1 can be pulled down by SH-130 but not by inactive SH-123. Moreover, SH-130 interrupted interaction between X-linked IAP/cIAP-1 and Smac. In a nude mouse xenograft model, SH-130 potently sensitized the DU-145 tumors to X-ray radiation without increasing systemic toxicity. The combination therapy suppressed tumor growth more significantly than either treatment alone, with over 80% of complete tumor regression. Furthermore, SH-130 partially blocked tumor necrosis factor-α- and radiation-induced nuclear factor-κB activation in DU-145 cells.

Conclusions: Our results show that small-molecule inhibitors of IAPs can overcome apoptosis resistance and radiosensitize human prostate cancer with high levels of IAPs. Molecular modulation of IAPs may improve the outcome of prostate cancer radiotherapy.

Androgen-independent disease is the main obstacle to improved survival and quality of life in patients with advanced prostate cancer. There is an urgent need for novel therapeutic strategies to overcome radioresistance in the treatment of advanced prostate cancer by specifically targeting the fundamental molecular basis of androgen-independent prostate cancer.

Authors' Affiliations: Departments of [1]Radiation Oncology, [2]Internal Medicine, and [3]Urology, University of Michigan Comprehensive Cancer Center, Ann Arbor, Michigan

Received 1/23/08; revised 6/13/08; accepted 7/5/08.

Grant support: Department of Defense Prostate Cancer Research Program grants W81XWH-04-1-0215 and W81XWH-06-1-0010 and NIH grant R01 CA121830-01 and R21 CA128220-01 (L. Xu) and NIH through the University of Michigan Cancer Center support grant 5 P30 CA46592. J. DeSano is a University of Michigan Undergraduate Research Opportunity Program student.

The costs of publication of this article were defrayed in part by the payment of page charges. This article must therefore be hereby marked *advertisement* in accordance with 18 U.S.C. Section 1734 solely to indicate this fact.

Note: Supplementary data for this article are available at Clinical Cancer Research Online (http://clincancerres.aacrjournals.org/).

Requests for reprints: Liang Xu, Division of Cancer Biology, Department of Radiation Oncology, University of Michigan Comprehensive Cancer Center, Room 4131, 1331 East Ann Street, Ann Arbor, MI 48109-0582. Phone: 734-615-7017; Fax: 734-615-3422; E-mail: liangxu@umich.edu.

©2008 American Association for Cancer Research.

doi:10.1158/1078-0432.CCR-08-0188

Most of the current anticancer therapies work, at least in part, through inducing apoptosis in cancer cells, including ionizing irradiation (1). Lack of appropriate apoptosis due to defects in the normal apoptosis machinery plays a crucial role in the resistance of cancer cells to a wide variety of current anticancer therapies. Radioresistance markedly impairs the efficacy of cancer radiotherapy and involves antiapoptotic signal transduction pathways that prevent radiation-induced cell death (2). The aggressive cancer cell phenotype is the result of a variety of genetic and epigenetic alterations leading to deregulation of intracellular signaling pathways, including an impaired ability of the cancer cell to undergo apoptosis (3). Primary or acquired resistance of hormone-refractory prostate cancer to current treatment protocols has been associated with apoptosis resistance in cancer cells and is linked to therapy failures (4, 5).

Current and future efforts toward designing new therapies to improve survival rates and quality of life for cancer patients will include strategies that specifically target cancer cell resistance to apoptosis. The inhibitors of apoptosis proteins (IAP) is an important class of intrinsic cellular apoptosis inhibitors (6, 7). IAPs potently suppress apoptosis against a large variety of apoptotic stimuli, including chemotherapeutics, radiation, and immunotherapy in cancer cells (8). The IAPs function as potent endogenous apoptosis inhibitors by directly binding to and effectively inhibiting three members of the caspase family of

Downloaded from http://aacrjournals.org/clincancerres/article-pdf/14/23/7701/1978518/7701.pdf by guest on 31 January 2023

Translational Relevance

Despite initial response to local therapy with surgery or radiation, many prostate cancer patients experience recurrence with advanced disease. Androgen ablation therapy produces only temporary responses because of the development of androgen independence. Failure to respond to radiation represents a critical problem in radiotherapy of hormone-refractory human prostate cancer. HRPC is resistant to apoptosis and IAPs have been shown to play a key role in apoptosis resistance. This study aims to investigate the radiosensitizing potential of a novel small-molecule IAP inhibitor both *in vitro* and *in vivo* in androgen-independent prostate cancer and the possible mechanism of radiosensitization. Our results show that the small-molecule IAP inhibitor radiosensitizes HRPC partly due to the enhanced apoptosis and inhibition of NF-κB induced by radiation. The data suggest that functional down-modulation of IAPs may be a promising approach for overcoming radiation resistance of HRPC. More importantly, the success of this strategy will pave the way to develop the small-molecule IAP inhibitors as an entirely new class of anticancer therapy for radiosensitizing human prostate cancer. The combination of IAP targeting molecular therapy and conventional radiotherapy may become a promising novel strategy to enhance the radiation efficacy and ultimately improve the survival of HRPC patients.

enzymes: two effector caspases (caspase-3 and -7) and one initiator caspase-9 (9). The X-linked IAP (XIAP) is perhaps the best characterized IAP member due to its potent activity (10). XIAP effectively inhibits both intrinsic and extrinsic apoptosis pathways by binding and inhibiting both initiator and effector caspases, whose activity is crucial for the execution of apoptosis (7, 11). Because effector caspase activity is both necessary and sufficient for irrevocable programmed cell death, XIAP functions as a gatekeeper to this final stage of the process. XIAP is widely expressed in cancer cell lines and tumor tissues and a high level of XIAP makes cancer cells apoptosis-resistant to a wide variety of therapeutic agents (12). cIAP-1/2 also inhibits both caspase-3 and caspase-7 although not as powerfully as XIAP (13).

Most components of the major cell death regulatory pathways have been implicated in radiation-induced cell death (14). It has been well established that IAPs, which are highly expressed in many types of cancer, including prostate cancer, appear to play a pivotal role in resistance to apoptosis induced by cancer therapy. Accumulating evidences show that XIAP and cIAP-1, two IAP members that are mostly studied for antiapoptosis and cell survival signaling, play a crucial role in chemoresistance or radioresistance (7). Specifically, radiation triggers apoptosis mediated by mitochondria, resulting in the release of mitochondrial proteins into cytoplasm, including Smac (15). The released Smac binds to XIAP and other IAP proteins and abolishes their antiapoptotic function. Because IAPs block apoptosis at the downstream effector phase, a point where multiple apoptosis signaling pathways converge, strategies targeting IAPs may prove to be highly effective in overcoming apoptosis resistance of human prostate cancer overexpressing IAPs. This link between radiation resistance and IAPs is supported by recent studies in which the suppression of XIAP levels by RNA interference or antisense indeed sensitized XIAP-overexpressing cancer cells to death receptor-induced apoptosis as well as radiation (16, 17).

Smac-based peptide inhibitors effectively overcome apoptosis resistance in different types of cancer cells with high levels of IAP and sensitize cancer cells to current therapeutic agents *in vitro* and *in vivo*, providing an important proof-of-concept for molecular therapy targeting IAPs (15, 18). Recently, we have designed Smac peptido-mimetics and nonpeptidic mimetics (Smac-mimetics) based on Smac peptide and the high-resolution experimental three-dimensional structures of Smac in complex with the XIAP BIR3 domain, called SH compounds (19, 20). These Smac mimetics are cell-permeable and have a much higher binding affinity to XIAP than the natural Smac peptide. Our preliminary results with newer and more potent Smac-mimetic IAP inhibitors show a 1 to 20 nmol/L binding affinity to XIAP BIR3 as well as potent cellular activity. These studies provide us with a solid foundation to determine if the IAPs are valid molecular targets for radiosensitization of human prostate cancer with IAP overexpression.

In this study, we evaluated the radiosensitizing effects of one of the Smac-mimetic IAP inhibitors, SH-130, in human prostate cancer cells with high levels of IAPs. We hypothesized that a Smac-mimetic targeting the IAP family of proteins would be highly effective in overcoming prostate cancer resistance to radiation therapy. We also investigated the potential molecular targets and mechanisms involved in the SH-130-mediated radiosensitization.

Materials and Methods

Reagents. Smac-mimetic compound SH-130, its negative control compound SH-123, and their biotin-labeled derivatives were dissolved in DMSO, stored as small aliquots at -20°C, and then diluted as needed in a cell culture medium. Recombinant human tumor necrosis factor-α (TNF-α) was obtained from Roche Applied Science. MG132 was provided by Biomol. High-glucose DMEM, fetal bovine serum, penicillin, streptomycin, and LipofectAMINE 2000 were purchased from Invitrogen. Pan-caspase inhibitor zVAD, caspase-3 substrate DEVD-AFC, and anti-Smac polyclonal antibody were purchased from Biovision. Crystal violet and β-actin antibody were purchased from Sigma-Aldrich. Antibodies against poly(ADP-ribose) polymerase (PARP), pro-caspase-3, p65/RelA, IκBα, and β-tubulin were purchased from Santa Cruz Biotechnology. Anti-XIAP and cIAP-1/2 antibodies were purchased from BD Biosciences. Survivin antibody was supplied by Novus Biologicals.

Cell culture. Human prostate cancer cell lines PC-3 and DU-145 and human normal fibroblast cell line WI-38 were purchased from the American Type Culture Collection. Luciferase stably transfected DU-145 cells ($DU\text{-}145^{Lux}$) were established as described previously (21). All types of cell lines were routinely cultured in high-glucose DMEM supplemented with 10% fetal bovine serum in a 5% CO_2 humidified incubator at 37°C. All media were also supplemented with 100 units/mL penicillin and 100 μg/mL streptomycin. Human normal prostate epithelial cell line PrEC was purchased from Lonza and maintained following the manufacturer's instruction.

Clonogenic cell survival assay. DU-145 cells were seeded in six-well plates at different cell densities (100-10,000 per well) and treated with SH-130 or SH-123 and X-ray radiation individually or in combination.

Downloaded from http://aacrjournals.org/clincancerres/article-pdf/14/23/7701/1978518/7701.pdf by guest on 31 January 2023

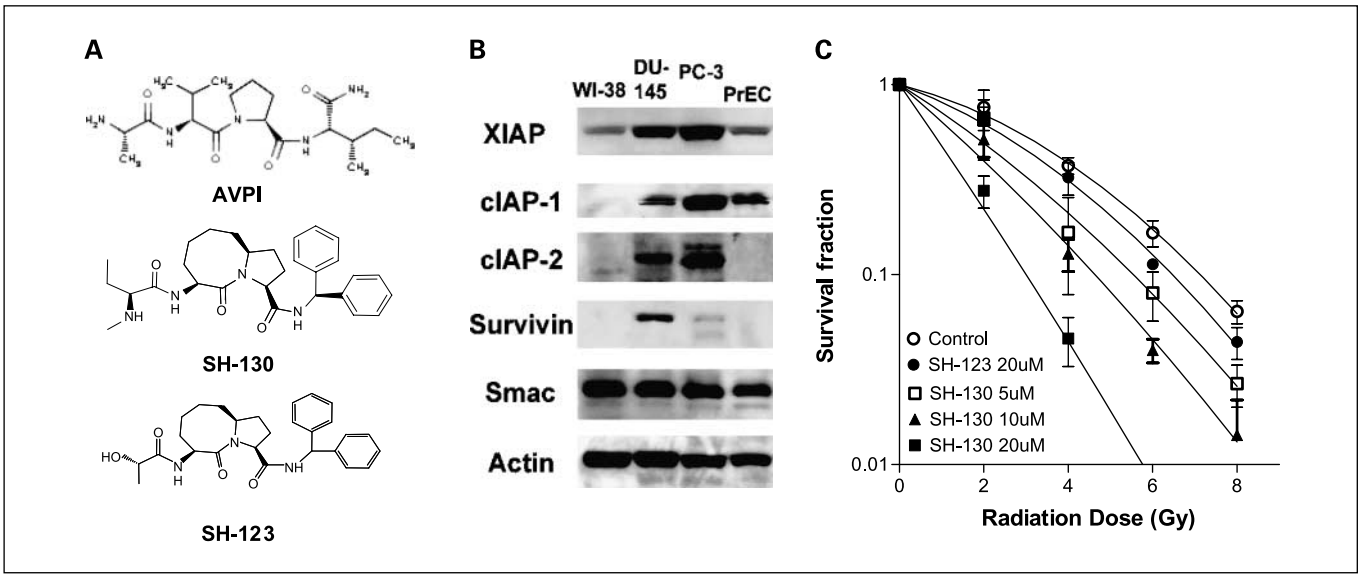

Fig. 1. *A,* structure of the Smac-mimetic compound SH-130 and an inactive control compound, SH-123. *B,* Western blot analysis of the expression of IAPs in human prostate cancer cells DU-145 and PC-3, with normal prostate epithelial cells PrEC and human fibroblast WI-38. *C,* SH-130-mediated radiosensitization of DU-145 cells by clonogenic survival assay. Cells seeded in six-well plates were treated with 5, 10, or 20 μmol/L SH-130 or 20 μmol/L SH-123, respectively, followed by 2, 4, 6, or 8 Gy X-ray radiation within 1 h. Each sample was tested in triplicate. After 14 d of incubation, colonies were stained by crystal violet and counted manually. Data were normalized and expressed as mean ± SD (n = 3). One of three independent experiments.

Solvent DMSO was used as a vehicle control. Each sample was tested in triplicate, and the cell medium was replaced 7 days later. After another 5 to 7 days of incubation, the plates were gently washed with PBS and stained with a 0.1% crystal violet solution. Colonies with over 50 cells were manually counted. The cell survival enhancement ratio was calculated as we described previously (22).

Western blot analysis. To determine the levels of protein expression in prostate cancer cell lines, cells were harvested and lysed in a radioimmunoprecipitation assay lysis buffer [50 mmol/L Tris-HCl (pH 8.0), 150 mmol/L NaCl, 0.1% SDS, 1% NP-40, 0.25% sodium deoxycholate, and 1 mmol/L EDTA] with freshly added protease inhibitor cocktail (Roche) for 15 min on ice and then centrifuged at 13,000 rpm for 10 min. Whole-cell extract was measured for total protein concentration using Bradford reagent (Bio-Rad), and proteins were resolved by SDS-PAGE (Bio-Rad). For nonreducing and non-denaturing SDS-PAGE, samples were mixed with loading buffer (no reducing agent) and directly loaded on a gel without boiling. After electrophoresis, the proteins were electrotransferred to nitrocellulose membranes (Bio-Rad), probed with the relevant primary antibody followed by horseradish peroxidase-conjugated secondary antibody (Pierce), and detected with the SuperSignal West Pico chemiluminescence substrate (Pierce). Intensity of the desired bands was analyzed using TotalLab software (Nonlinear Dynamics).

Apoptosis assay. To detect apoptosis, we used an Annexin V-FITC and propidium iodide double staining kit (Trevigen). In brief, DU-145 cells were seeded into six-well plates and treated with SH-130 or negative control SH-123 with or without pretreatment with the pan-caspase inhibitor zVAD (Biovision). X-ray irradiation was done immediately after drug addition. Twenty-four hours after radiation, the cells were collected, gently washed twice with cold PBS, stained with Annexin V and propidium iodide as per manufacturer's instruction, and analyzed with a flow cytometer (FACSCalibur; BD Biosciences) in the Flow Cytometry Core at the University of Michigan Cancer Center. Other aliquoted samples were processed for caspase function and Western blot analysis.

Caspase-3 function assay. Caspase activation of treated DU-145 cells was determined following the instructions of a caspase-3 detection kit (BioVision). Cells were lysed in a lysis buffer, and whole-cell lysates (20 μg) were incubated with 25 μmol/L fluorogenic substrate DEVD-AFC in a reaction buffer (containing 5 mmol/L DTT) at 37°C for 2 h. Proteolytic release of AFC was monitored at λ_{ex} = 405 nm and λ_{em} = 500 nm using a microplate reader (BMG Labtech). Fold increase of the fluorescence signal was calculated for each treated sample by dividing its normalized signal activity by that of the untreated control.

Pull-down and immunoprecipitation assay. DU-145 cells were washed with ice-cold PBS, harvested, and resuspended in a lysis buffer

Table 1. Radiobiological variables from surviving curves

	Mean inactivation dose	Enhancement ratio	Survival fraction (2 Gy)	Gy (1%)
Control	3.66		0.70	10.83
SH-123 (20 μmol/L)	2.96	1.24	0.57	10.49
SH-130 (5 μmol/L)	2.53	1.45	0.49	9.53
SH-130 (10 μmol/L)	2.05	1.79	0.40	8.42
SH-130 (20 μmol/L)	1.28	2.86	0.21	5.63

NOTE: Radiobiological variables were calculated from survival curves in Fig. 1C based on linear-quadratic model. Enhancement ratio was calculated from mean inactivation dose in control group divided by that in treated group. Gy (1%), radiation dose leading to 1% cell survival.

Downloaded from http://aacrjournals.org/clincancerres/article-pdf/14/23/7701/1978518/7701.pdf by guest on 31 January 2023

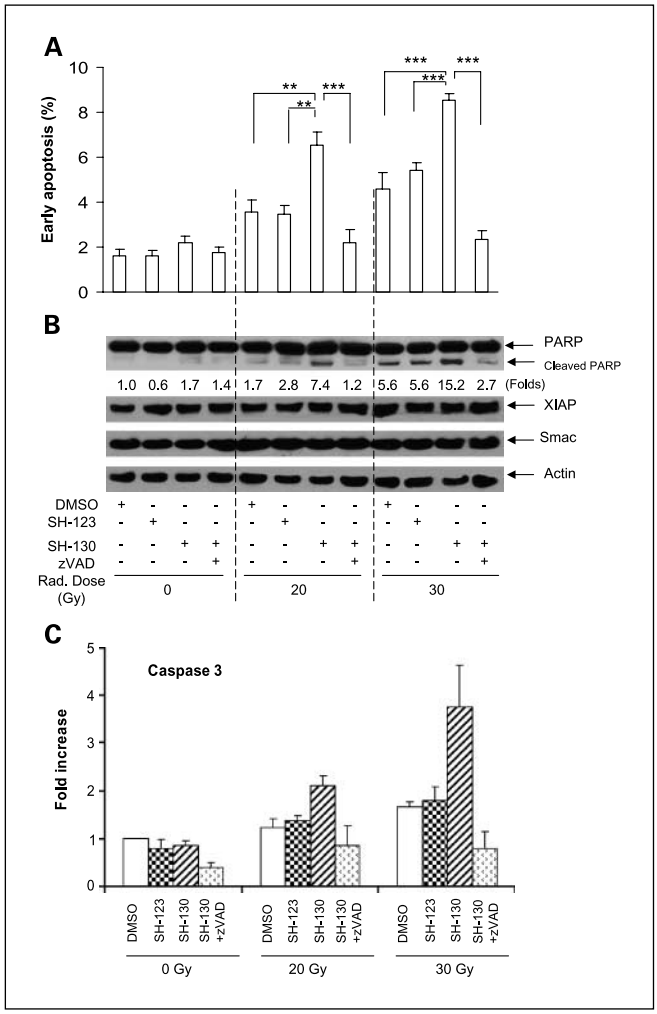

Fig. 2. SH-130 enhances radiation-induced apoptosis. DU-145 cells were seeded into six-well plates at the concentration of 2×10^5/mL, pretreated with zVAD (2.5 μmol/L) for 1 h, incubated with 10 μmol/L SH-130 or SH-123, and irradiated at doses of 0, 20, or 30 Gy, respectively. Twenty-four hours after incubation, cells were harvested and processed for further detection. One of three independent experiments. *A,* early apoptotic cell populations after treatment. DU-145 cells were stained with Annexin V-FITC and propidium iodide (Trevigen) and determined by flow cytometry. Mean ± SD ($n = 3$). **, $P < 0.01$; ***, $P < 0.001$, Student's t test. *B,* Western blot analysis of apoptosis-related proteins. Samples were probed with antibodies against PARP, caspase-3, XIAP, and Smac. Actin is shown as a loading control. Band intensity of cleaved PARP was normalized to actin. *C,* caspase-3 activation after treatment. Whole-cell lysates (20 μg) were reacted with fluorogenic substrate DEVD-AFC. After incubation at 37°C for 2 h, released AFC was monitored by a microplate reader (BMG Labtech). Mean ± SD ($n = 3$). Fold increase of fluorescence signal was expressed by normalizing activity to untreated control.

[50 mmol/L Tris-HCl (pH 7.5), 150 mmol/L NaCl, 1% NP-40, 0.5% sodium deoxycholate, and protease inhibitor tablet (Roche)]. For pull-down assay, after preclearing the streptavidin agarose gel (Invitrogen) at 4°C for 2 h, whole-cell lysate (1 mg total proteins) was incubated with biotin-labeled SH-130 (20 μmol/L) with or without the addition of an unlabeled SH-130 competitor (200 μmol/L). DMSO was used as a solvent control. After rotation at 4°C for 3 h, the lysate was incubated overnight with the gel (50 μL) at 4°C. For immunoprecipitation assay, the lysate (1 mg total proteins) was incubated with 1 and 10 μmol/L SH-130 or 10 μmol/L SH-123 at 4°C for 1 h. Antibody (10 μL) was then added, and the sample was incubated for 1 h before an overnight incubation with 50 μL protein A/G-agarose gel (Invitrogen). The immunoprecipitates were washed five times with desired wash buffer (Roche), eluted with SDS-PAGE sample buffer, and analyzed by Western blot.

Animal studies. The general procedure for *in vivo* experiments was described previously (22). Briefly, female athymic NCr-*nu*/*nu* nude mice (5-6 weeks old) were inoculated s.c. on both sides of the lower back above the tail with 3×10^6 per 0.2 mL DU-145 cells. When tumors reached 50 to 100 mm^3, the mice were randomized into four groups (8 mice per group) and treated with either SH-130 i.v. injected with 50 mg/kg for q.d. × 5 × 2 weeks, X-ray irradiation with 2 Gy daily for q.d. × 5 × 2 weeks, or a combination of SH-130 and radiation. The vehicle control and radiation-only groups received the same amount of DMSO solvent. Tumor size and body weight were measured twice a week. Tumor volume was calculated using the formula: $V = a \times b^2 / 2$, where a and b represented both the long and the vertical short diameter of the tumor. For *in vivo* imaging experiments, mice were transplanted s.c. with 5×10^6 cells per 0.2 mL DU-145^{Lux} cells. Treatment started (day 0) when the average tumor volume reached 50 mm^3 using the following regimen: SH-130 50 mg/kg i.v. q.o.d. × 3 weeks, X-ray irradiation 2 Gy q.d. × 5 × 3 weeks, or a combination of SH-130 and radiation. On days 0, 8, 17, 24, 41, and 120, mice were imaged 12 min after i.p. injection of luciferin using the Xenogen Bioluminescence Imaging (BLI) System in the University of Michigan Small Animal Imaging Core. Light intensity was quantified using LivingImage software on a red (high intensity/cell number) to blue (low intensity/cell number) visual scale. All animal experiments were done according to protocols approved by the University of Michigan Committee for Use and Care of Animals.

Nuclear factor-κB activity assay. Two independent assays were done to determine the effect of SH-130 on TNF-α-induced nuclear factor-κB (NF-κB) activation as shown below.

NF-κB reporter assay. DU-145 cells were seeded into a 24-well plate 24 h before transfection. For each well, cells were transiently cotransfected with 0.4 μg of a NF-κB reporter construct (pNF-κB; Panomics) or a control reporter plasmid (pControl; Panomics), together with 0.2 μg of a β-galactosidase reporter vector (Promega), which was used to normalize NF-κB reporter gene activity, using LipofectAMINE 2000 (Invitrogen). Twenty-four hours after transfection, cells were pretreated with SH-130 with or without the caspase inhibitor zVAD or SH-123 for 1 h followed by TNF-α stimulation for 4 h. The proteasome inhibitor MG132 was used as a positive control. Cell lysates were prepared using Reporter Lysis Buffer (Promega). For luciferase and β-galactosidase assays, the samples were measured on a microplate luminometer (BMG Labtech) using the Bright-Glo luciferase kit (Promega) and β-galactosidase enzyme assay kit (Promega), respectively, according to the manufacturer's instructions. Fold increase was calculated for each treated sample by dividing normalized luciferase activity by that of the untreated control.

Quantitative real-time PCR. Quantitative PCR was done to determine the expression level of the TNF gene as a NF-κB target gene (23). Total RNA was extracted from DU-145 cells using TRIzol reagent (Invitrogen) according to the manufacturer's instructions. Reverse transcription reaction with 1 μg total RNA in 100 μL was done following the instructions of the TaqMan Reverse Transcription Kit (Applied Biosystems). For quantitative PCR, FAM probe TNF primer (Applied Biosystems) was used for detection of target gene expression, and SYBR Green-labeled actin (Applied Biosystems) was used as an internal control, with the primers designed as forward 5′-ATGCAGAAG-GAGATCACTGC-3′ and reverse 5′-TCATAGTCCGCCTAGAAGCA-3′. All reactions with TaqMan PCR Master Mix (Applied Biosystems) were done on the Mastercycler realplex system (Eppendorf). Fold increase of gene expression was calculated for each treated sample by dividing normalized TNF expression activity with that from the untreated control.

Statistical analysis. Two-tailed Student's t test and two-way ANOVA were employed to analyze the *in vitro* and *in vivo* data, respectively, using Prism 5.0 software (GraphPad Prism). A threshold of $P < 0.05$ was defined as statistically significant.

Downloaded from http://aacrjournals.org/clincancerres/article-pdf/14/23/7701/1978518/7701.pdf by guest on 31 January 2023

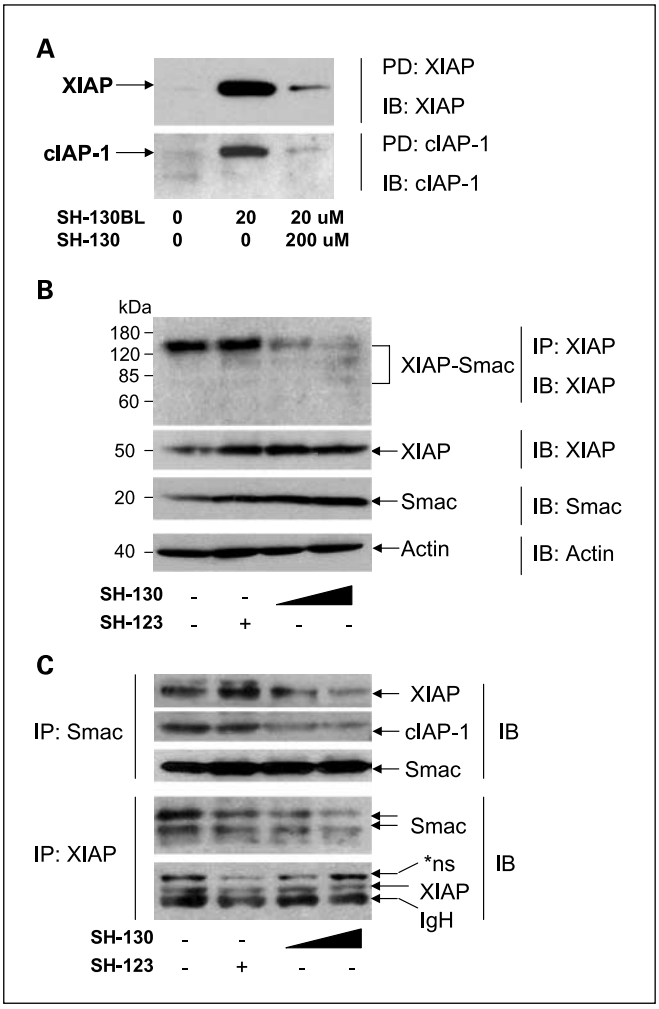

Fig. 3. SH-130 interrupts interaction between XIAP/cIAP-1 and Smac. DU-145 cells were collected and disrupted in a lysis buffer. Pull-down or immunoprecipitation was done as described in Materials and Methods. Immunoprecipitates were analyzed by Western blot. Endogenous XIAP, cIAP-1, and Smac were visualized by relevant antibodies. *A,* biotin-labeled SH-130 (SH-130BL) was incubated with cell lysates with or without nonlabeled SH-130 followed by incubation with precleared streptavidin-agarose beads. *B,* cell lysates were incubated with 1 and 10 μmol/L SH-130 or 10 μmol/L SH-123 for 1 h. Lysates were mixed with a sample buffer (Bio-Rad; without reducing agent) and directly analyzed by Western blot without boiling. Actin was used as a loading control. *C,* cell lysates from *B* were incubated with an anti-Smac or an anti-XIAP antibody and mixed with protein A/G-agarose beads. Eluents were analyzed by Western blot and probed with specified antibodies. IgG heavy chain (*IgH*) was probed as a control. One of three independent experiments. *PD,* pull-down; *IP,* immunoprecipitation; *IB,* immunoblotting; *ns,* nonspecific.

Results

Synergistic induction of radiation-induced cancer cell growth inhibition by the small-molecule IAP inhibitor. As reported previously (19, 20), a series of compounds were designed to mimic AVPI, the critical NH_2-terminal tetrapeptide on the active Smac protein (Fig. 1A). SH-130, a lead compound of these Smac-mimetics, was found to be 20 to 30 times more potent in binding to XIAP than the cell-permeable Smac peptide pSMAC-8c, a positive control for serial SH compounds used previously (Fig. 1A). Another analogue, SH-123, which was almost 1,000 times less active than SH-130, was used as an inactive control (Fig. 1A). Human prostate cancer DU-145 and PC-3 cell lines have medium to high levels of most of IAPs, whereas the normal human fibroblast cell line WI-38 and normal human prostate epithelial cells PrEC show low levels of IAPs (Fig. 1B).

To determine whether the Smac-mimetic compound could potentiate radiation-induced inhibition of cancer cell growth, we examined the radiosensitization of SH-130. SH-130 promoted radiation-induced clonogenic cell death dose-dependently, whereas SH-123 exhibited much less effect even at a high dose (Fig. 1C). Radiobiological variables were calculated and summarized in Table 1. The radiosensitizing activity of SH-130 was not observed in normal cells PrEC and WI-38 that have low IAPs (data not shown). We have also carried out MTT-based cytotoxicity assay (22) and SH-130 alone showed IC_{50} > 100 μmol/L in prostate cancer DU-145 and PC-3 cells as well as WI-38 cells, indicating that SH-130 is not a cytotoxic compound, consistent with other small-molecule Smac-mimetics we reported earlier (19, 20).

Enhancement of radiation-induced apoptosis by inhibition of IAPs. Preliminary data indicated that in cell-free systems SH-130, but not SH-123, abolished the inhibitory action of IAPs on both caspase-9 and caspase-3 in a dose- and time-dependent manner, showing a potent effect on competing IAPs and thus activating caspases. To provide further evidence for the role of SH-130 in mediating radiation-induced apoptosis, DU-145 cells were treated with SH-130 or SH-123 with or without X-ray radiation. As shown in Fig. 2A, induction of early apoptotic events (Annexin V positive) became evident when cells were treated with either 20 or 30 Gy together with 10 μmol/L SH-130. A 4- to 5-fold increase was seen compared with the untreated control and a 2-fold increase over radiation alone ($P < 0.01$). Pretreatment with the pan-caspase inhibitor zVAD abolished this increase in radiation-induced early apoptosis by SH-130 ($P < 0.001$; Fig. 2A), indicating that SH-130-mediated radiosensitization is caspase dependent. In contrast, neither SH-130 nor SH-123 alone induced significant apoptosis, suggesting a nontoxic profile of these compounds. We also evaluated total (early plus late) apoptotic events and obtained similar results (Supplementary Fig. S1). Furthermore, in the cells treated with radiation plus SH-130, a clear PARP cleavage was observed (Fig. 2B) compared with the cells treated with radiation alone. Because PARP is one of the substrates of caspase-3, our functional assay also showed similar profile on caspase-3 activation (Fig. 2C). Here again, zVAD efficiently blocked the SH-130 effect on caspase-3 activation and PARP cleavage. For all the samples tested (Fig. 2B), the expression level of XIAP and Smac did not change significantly, indicating that SH-130 acts on the apoptosis pathway, not by inhibiting the expression of IAPs.

Blockade of XIAP/cIAP-1 and Smac interaction by the IAP inhibitor. To further examine whether the small-molecule IAP inhibitor, SH-130, binds to the IAP family of proteins in cells as designed, we carried out IAP pull-down assays using biotin-labeled compounds. SH-130 was labeled with biotin (SH-130BL) via chemical synthesis. A fluorescence polarization-based binding assay confirmed that SH-130BL had the same binding affinity to XIAP as unlabeled SH-130.[4] SH-130BL successfully pulled down both XIAP and cIAP-1 in DU-145 cells

[4] Data not shown.

Downloaded from http://aacrjournals.org/clincancerres/article-pdf/14/23/7701/1978518/7701.pdf by guest on 31 January 2023

(Fig. 3A). Competition with unlabeled SH-130 effectively blocked the pull-down of both XIAP and cIAP-1 by SH-130BL. Furthermore, we conducted immunoprecipitation assays to see if SH-130 interfered with XIAP (or cIAP-1) and Smac interaction. Interestingly, under nonreducing and nondenaturing conditions, XIAP and Smac formed a complex at molecular weight ranging from ~80 to 160 kDa (Fig. 3B), consistent with the tetramer model (24). XIAP-Smac complex levels were decreased by the addition of SH-130, but not SH-123, with increasing levels of free XIAP and Smac (Fig. 3B). Furthermore, SH-130 dose-dependently interrupted interaction between Smac and XIAP or cIAP-1 (Fig. 3C). Interestingly, when mature Smac was pulled down together with XIAP, two bands always seemed to be visualized by Western blot (Fig. 3C). The upper band (~28 kDa) level showed the same alteration as the lower band (~21 kDa), which is thought to be the cleaved or activated Smac. Compared with the artificial transfection with tag-labeled system (25), our condition is more likely to mimic the native intracellular protein behavior. These data confirm that the IAP inhibitors can bind to XIAP/cIAP-1, thus interrupting the interaction between endogenous XIAP/cIAP-1 and Smac in prostate cancer cells.

In vivo *tumor suppression effect of the IAP inhibitor with radiation.* To evaluate the radiosensitization potential of SH-130 *in vivo*, a DU-145 tumor model was established as we described previously (4, 22). The DU-145 tumors were resistant to radiation, and SH-130 alone did not show tumor suppression effect (Fig. 4A). However, SH-130 synergistically sensitized the DU-145 tumors to radiation without showing systemic toxicity (Fig. 4B). The combination therapy inhibited tumor growth significantly more effectively than either treatment alone ($P < 0.001$, $n = 14$), and no obvious animal toxicity was observed. Notably, 5 of 14 tumors in the combination group showed complete regression that did not grow back 5 months after the therapy, whereas the radiation-alone group had only 2 of 10 tumors with complete regression. No complete regression in the SH-130-alone or vehicle control groups was observed.

In the second experiment, we wished to extend the treatment period to a more clinically relevant 3-week course of therapy. For this experiment, we used the DU-145^{Lux} tumor model and employed BLI to evaluate tumor response. SH-130 plus radiation led to complete tumor regression (undetectable signal in BLI in Fig. 4C). By quantification, the combination therapy resulted in a 2-log reduction in bioluminescence signal compared with the radiation-alone group and a 4- to 5-log reduction compared with the vehicle control group (Fig. 4D). BLI was also conducted on days 0, 24, and 120 (Supplementary Fig. S2), and percentage of complete tumor regression is summarized in Fig. 4D. The percentage of complete tumor regression in the radiation-alone group was highest (35%) on day 41 and dropped to 33.3% on day 120, indicating tumor recurrence over time. For the combination therapy group, the

Downloaded from http://aacrjournals.org/clincancerres/article-pdf/14/23/7701/1978518/7701.pdf by guest on 31 January 2023

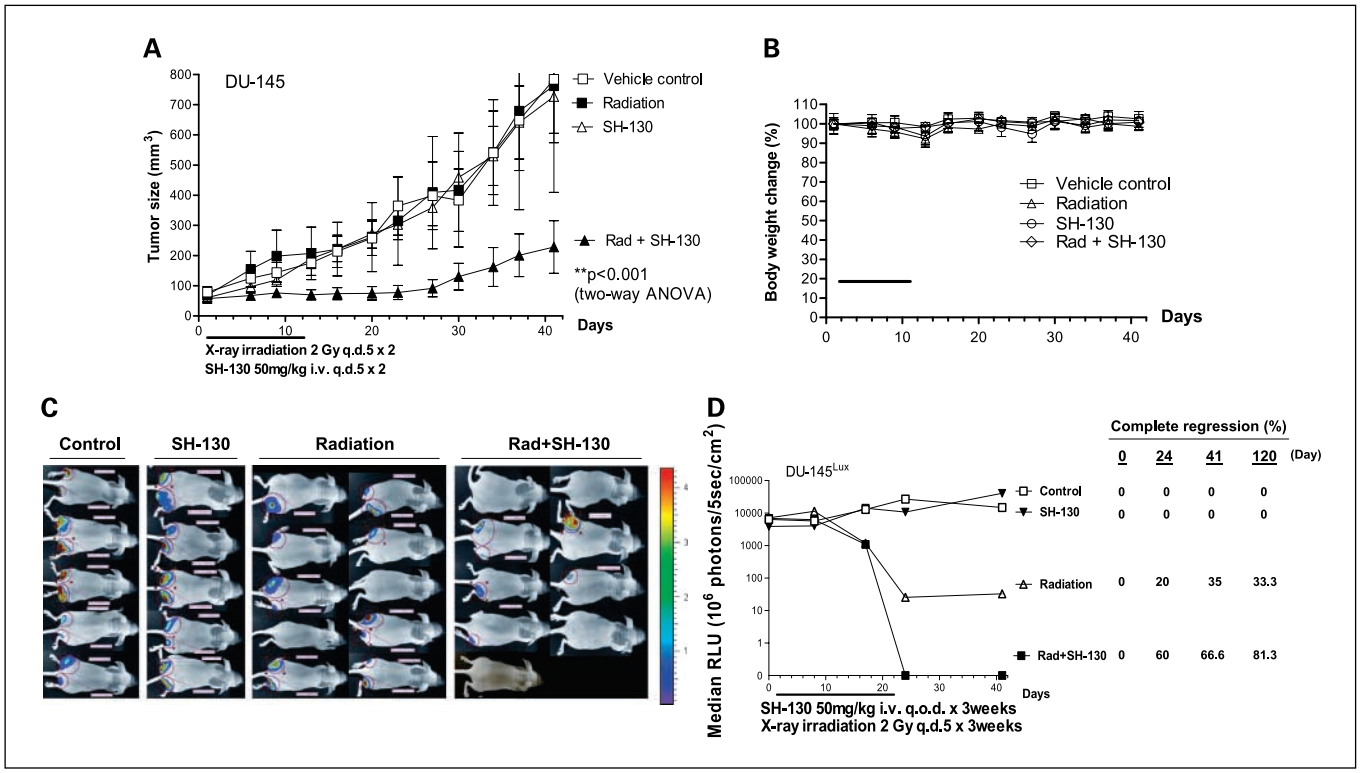

Fig. 4. SH-130 potentiates DU-145 tumor regression induced by X-ray radiation with caliper measurement (*A* and *B*) or BLI (*C* and *D*). Nude mice bearing DU-145 cells were treated with either SH-130, or X-ray irradiation, or a combination. Tumor size (*A*) and body weight (*B*) were measured twice a week, and curves were plotted up to day 41. Mean ± SE ($n = 16$) for tumor volume (*A*) and mean ± SE ($n = 8$) for body weight (*B*). *C* and *D*, SH-130 combined with radiation eradicated DU-145 tumors by BLI. Nude mice bearing DU-145^{Lux} cells were treated as described in Materials and Methods. Imaging was carried out to visualize bioluminescent tumors on days 0, 8, 17, 24, 41, and 120, respectively. *C*, BLI of DU-145^{Lux} on day 41. The light intensity of each photo was quantified to an optimized visual scale (from *red* to *blue*). *D*, summary of quantitative data of bioluminescence intensity. Absolute photon counts of tumors were measured and expressed as a median of relative light unit (*RLU*). Percentage of complete regression was calculated by dividing the number of eradicated tumors with total tumors. *Rad*, X-ray radiation.

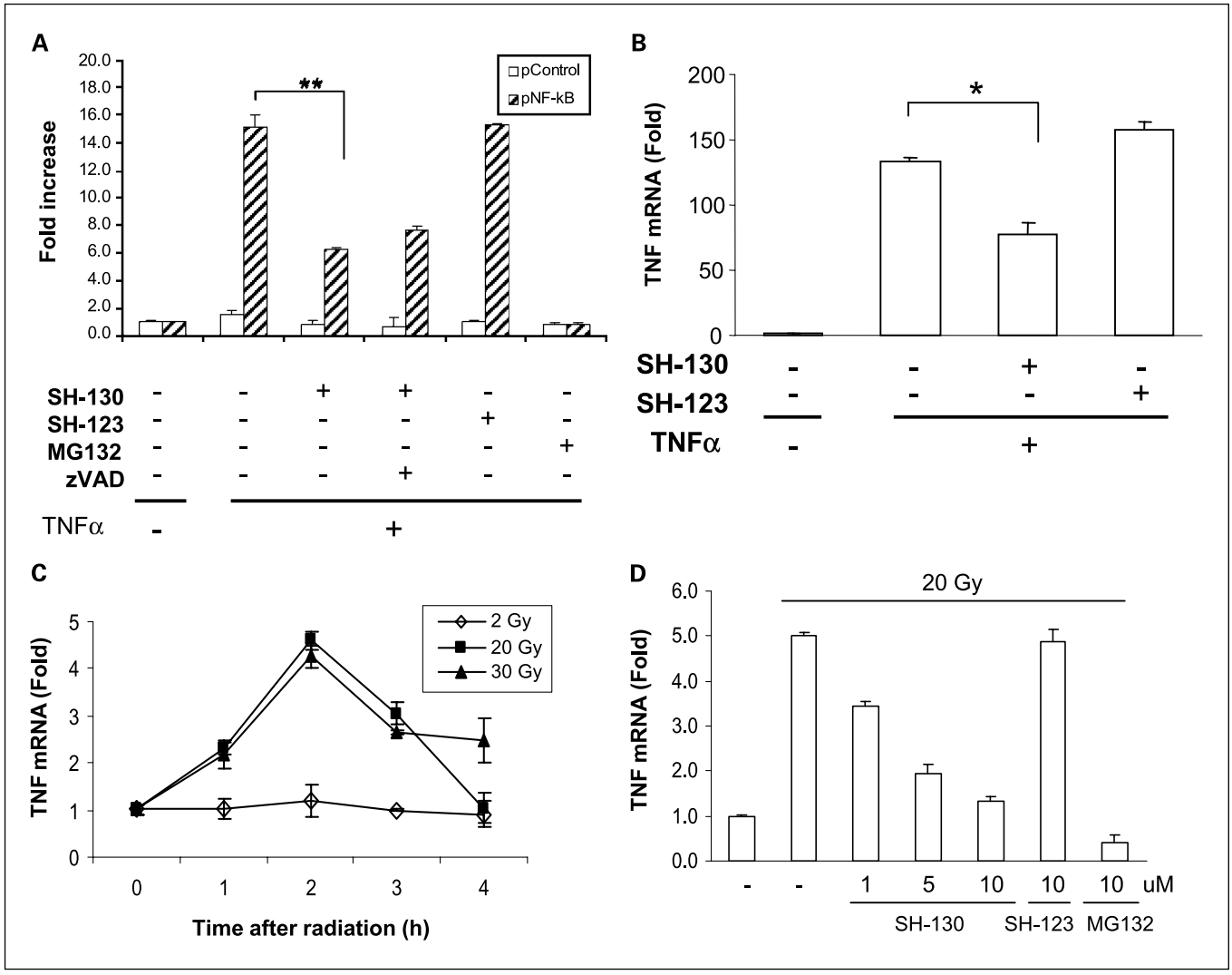

Fig. 5. SH-130 inhibits NF-κB activation induced by TNF-α (*A* and *B*) and radiation (*C* and *D*). *A,* DU-145 cells were transiently cotransfected with pNF-κB or pControl (0.4 μg/well) together with β-galactosidase plasmid (0.2 μg/well). Cells were then pretreated with SH-130 (20 μmol/L) with or without zVAD (2.5 μmol/L) or SH-123 (20 μmol/L) for 1 h followed by TNF-α stimulation for 4 h. MG132 (10 μmol/L) was used as a positive control. Luciferase and β-galactosidase activities were measured as described in Materials and Methods. Fold increase was calculated as mean ± SD ($n = 2$). One of three independent experiments. **, $P < 0.01$. *B,* cells were pretreated with 20 μmol/L SH-130 or SH-123 for 1 h before 10 min pulse stimulation of TNF-α. Total RNA was extracted and quantitative PCR was done as described in Materials and Methods. Fold increase was calculated by dividing the normalized TNF expression activity by that of the untreated control. *Columns,* mean; *bars,* SD ($n = 3$). *, $P < 0.05$. *C,* cells were irradiated with the indicated doses of X-ray radiation. TNF mRNA expression level at desired time points was detected and normalized as described in *B*. *D,* cells were pretreated with the indicated doses of compounds for 1 h and TNF mRNA expression level was determined 2 h after 20 Gy radiation. MG132, positive control.

percentage of complete tumor regression continued to increase up to day 120 (81.3%), indicating a potent and long-term efficacy of the combination treatment. Thus, two *in vivo* studies showed a similar and promising *in vivo* radiosensitization efficacy of the IAP inhibitor.

Suppression of NF-κB activation by inhibiting IAPs. To test the hypothesis that SH-130 may also work on the NF-κB pathway, we analyzed the effects of SH-130 on NF-κB activation induced by TNF-α and X-ray radiation in DU-145 cells. Using luciferase-based NF-κB reporter assay (26), SH-130 inhibited TNF-α-induced NF-κB activation by >50% ($P < 0.01$) and the inhibition could not be blocked by zVAD (Fig. 5A), indicating that the IAP inhibitor-mediated NF-κB inhibition is caspases independent. Moreover, SH-130 partially inhibited NF-κB activation, even at a high concentration, compared with MG132 (Fig. 5A). SH-130 inhibited TNF-α-induced IκBα degradation (Supplementary Fig. S3), yet without a significant change in RelA nuclear translocation (data not shown), suggesting that SH-130-mediated inhibition of NF-κB activation is indirect. Quantitative real-time PCR assay further confirmed that TNF gene expression was down-regulated 50% by SH-130 ($P < 0.05$), but not by negative control compound SH-123, after TNF-α stimulation (Fig. 5B), indicating that SH-130 clearly although partially blocked NF-κB target gene expression.

Next, we examined if SH-130 has similar suppression effect on X-ray radiation-induced NF-κB target gene expression. Radiation (20 Gy) was employed to trigger NF-κB activation as high radiation doses (20 and 30 Gy) exhibited activation of TNF gene expression by 4- to 5-fold more than low dose (2 Gy; Fig. 5C). Similar to TNF-α, radiation-induced TNF gene expression could also be partially suppressed by SH-130 in a

Downloaded from http://aacrjournals.org/clincancerres/article-pdf/14/23/7701/1978518/7701.pdf by guest on 31 January 2023

dose-dependent manner (Fig. 5D) compared with its negative analogue, SH-123. These data show that SH-130 can block both TNF-α- and radiation-induced NF-κB activation in terms of inhibiting NF-κB target gene expression.

Discussion

In this study, we have found that a small-molecule IAP inhibitor potently sensitizes prostate cancer DU-145 cells to X-ray irradiation and increases radiation-induced cell death and tumor growth delay both *in vitro* and *in vivo*. Such effects may be due to activation of the apoptosis pathway. Moreover, the IAP inhibitor SH-130 also blocked activation of the NF-κB partially and indirectly, suggesting a potential cross-talk between apoptosis and NF-κB pathways (Fig. 6). The data confirmed our hypothesis that molecular modulation of IAP family proteins may improve the outcome of prostate cancer radiotherapy and represents a promising molecularly targeted therapy for hormone-refractory prostate cancer.

Small-molecule inhibitors of IAPs are a promising choice for functionally blocking IAPs and overcoming chemoresistance/radioresistance of cancer cells with high levels of IAPs. Our previous studies showed that the Smac-mimetic tetrapeptide pSmac-8c (used as the positive control) significantly sensitized both androgen-independent DU-145 and PC-3 cells to chemotherapeutic agents (19, 20), indicating that IAP is a valid target for overcoming chemoresistance in prostate cancer cells, and our current study supports that modulating IAPs is a promising approach on radiosensitization. Future work will focus on comparing androgen-dependent LNCaP and its androgen-independent derivative cell line CL-1 on their response to radiation and SH-130. Expected data on this isogenic cell model will further support that IAPs may play an essential role in the transition from androgen-dependent to androgen-independent prostate cancer, and overcoming resistance of radiation-induced apoptosis can be achieved by down-regulating IAPs.

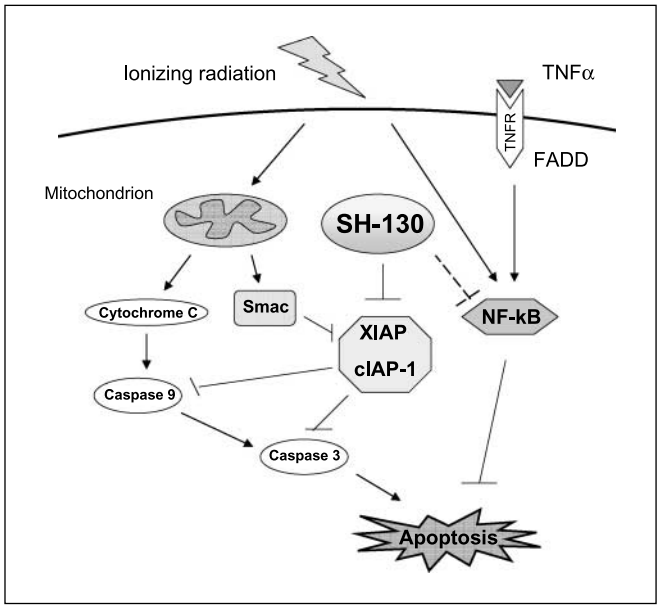

Fig. 6. Working model of the Smac-mimetic IAP inhibitors in radiosensitization. SH-130 enhances ionizing radiation-induced apoptosis via the intrinsic (mitochondrion) pathway by inhibiting XIAP/cIAP-1 activity and blocking caspase activation. On the other hand, SH-130 blocks NF-κB activation induced by TNF-α as well as ionizing radiation, indicating the suppression effect of radiation-mediated prosurvival signaling that attenuates apoptosis.

Our *in vivo* studies showed consistently that IAP inhibition exhibits promising radiosensitivity in the DU-145 xenografted model, although IAP inhibitor itself is nontoxic and shows no tumor suppression effect alone. Data from regular tumor volume measurement and BLI imaging are consistent in exhibiting a synergistic efficacy when SH-130 is used together with X-ray radiation. By BLI, mice in the combination group showed an increasing trend toward complete tumor regression that lasted up to 4 months after treatment, indicating the long-term tumor-suppressing efficacy of combination therapy over radiation alone. Using BLI for the efficacy study is critically important, especially when the tumor disappears as a complete tumor regression. Conventional tumor measurement by hand will still detect a scar or nodule, but no live tumor cells are detectable, as the BLI will detect no light emission. On the other hand, some tumors may appear to have completely disappeared and will not be detectable by hand, but BLI can still detect light emission and reveal the presence of live tumor cells. Therefore, the more sensitive and quantitative BLI will yield robust and quantitative efficacy data, especially when evaluating the complete tumor regression in the current study.

Ionizing radiation activates the NF-κB signaling pathway, and blocking this pathway can sensitize cancer cells response to radiation (27, 28). Classically, cytokines such as TNF-α trigger NF-κB activation, typically mediated by TNF receptor-associated factor 2. It has been shown that TNF receptor-associated factor 2 physically interacts with cIAP-1, another IAP protein that is commonly studied along with XIAP (29). In addition, embelin, a natural IAP inhibitor first reported by us (30), sequentially inhibits NF-κB activation at multiple levels (26). Moreover, XIAP could induce TAK1-dependent NF-κB activation (31). Thus, it is reasonable to postulate that IAPs may function as "bridging" molecules mediating cross-talk between apoptosis and NF-κB pathways. Our data show that SH-130 indeed inhibits NF-κB activation, partially and indirectly, by TNF-α and X-ray radiation. This partial effect of an IAP inhibitor on NF-κB activation is consistent with an earlier report showing that partial NF-κB inhibition by another class of Smac-mimetics (32). Inhibition of IκBα degradation by SH-130 reflects an effect at the level of the IκBα kinase complex as shown by embelin (26). Currently, we are delineating the detailed signaling pathways and molecules involved in the cross-talk either via cIAP-1 or XIAP. This may have important implications for the rational design of novel therapies targeting IAPs and optimal recruitment of the patient population that will benefit the most from such therapy.

DU-145 cells are highly resistant to radiation potentially due to high levels of IAPs as well as constitutive active NF-κB pathway (33). It is conceivable that the dose of radiation used might affect NF-κB activation as well as radiation-induced cell death, where the high and low doses may stimulate different cellular responses. In the clinic, the dose of radiation therapy on patients is 1.8 to 2 Gy daily fractionation with total doses of 20 to 70 Gy. Thus, in the current study, we followed the clinical regimen with totaling 20 and 30 Gy in two animal studies. Consistent with previous reports that a relative high dose (15-20 Gy) of X-ray radiation could induce NF-κB activation in

Downloaded from http://aacrjournals.org/clincancerres/article-pdf/14/23/7701/1978518/7701.pdf by guest on 31 January 2023

human tumor cells *in vitro* (34, 35), we found that, in our system, high-dose radiation (20 and 30 Gy) effectively induced apoptosis as well as NF-κB activation but not the low doses (2-4 Gy). Furthermore, RelA was clearly observed at doses >15 Gy (data not shown). Taken together, the radiosensitization effect of Smac-mimetic SH-130 is due, at least in part, to the simultaneous inhibition of IAPs and the NF-κB survival signaling pathway, which is constitutively active in androgen-independent prostate cancer cells.

Very recently, three groups reported that several Smac-mimetic IAP inhibitors can induce TNF-α-dependent apoptosis in sensitive cell lines via cIAP-1 down-regulation and NF-κB activation (36–38). However, most of the androgen-independent prostate cancer cells are resistant to TNF-α and have constitutive active NF-κB signaling (33). How these resistant cancer cells respond to IAP inhibitors remains to be investigated. In our hands, those cells, including DU-145, PC-3, and CL-1, are highly resistant to our Smac-mimetic IAP inhibitors such as SH-130, which has a IAP-binding affinity comparable with that of the compounds used in the three reports (36–38). To our knowledge, this is the first report that an IAP inhibitor blocks radiation-induced NF-κB activation in these TNF-α-resistant cells. Moreover, SH-130 treatment does not induce cIAP-1 down-regulation, TNF-α up-regulation, and NF-κB activation in these resistant cells (Supplementary Fig. S4). This mode of action is distinct from that in TNF-α-sensitive cells reported recently (36–38). Our study has significant clinical implications and provides important impetus for using IAP inhibitors as an adjuvant therapy for the TNF-α-resistant, NF-κB constitutively active cancers that account for the majority of patients who are refractory to conventional therapy.

In conclusion, our data provide strong support that modulating IAPs may be a promising novel approach to radiosensitization of human prostate cancer, especially among hormone-refractory, locally advanced, high-risk patients. In a clinical context, although hormone-refractory prostate cancer still exerts response to high-dose palliative radiation therapy to achieve the local control in patients (39), the patient population that could benefit the most would be those with a high Gleason score (>8) and high prostate-specific antigen (>20) without metastatic disease and with a high failure rate even with high-dose radiation. Showing a reasonable relevance to prostate cancer therapy in clinic, our reported small-molecule IAP inhibitor has a promising implication on overcoming radiation resistance of human prostate cancer with high levels of IAPs.

Disclosure of Potential Conflicts of Interest

L. Xu is coinventor of the related compound.

Acknowledgments

We thank Drs. Dian Wang, Jiaxin Zhang, and Mu Li for technical support in the experiments; Dr. Shaomeng Wang for kindly providing IAP inhibitors in our study; Dr. Lori Roberts (University of Michigan Comprehensive Cancer Center Unit of Laboratory Animal Medicine) for measuring tumor sizes; Susan Harris for help with the article; the University of Michigan Comprehensive Cancer Center Flow Cytometry Core for flow cytometry analysis; and the University of Michigan Biomedical Imaging Core for BLI of animals.

References

1. Szostak MJ, Kyprianou N. Radiation-induced apoptosis: predictive and therapeutic significance in radiotherapy of prostate cancer [review]. Oncol Rep 2000;7:699–706.
2. Lawrence TS, Davis MA, Hough A, Rehemtulla A. The role of apoptosis in 2′,2′-difluoro-2′-deoxycytidine (gemcitabine)-mediated radiosensitization. Clin Cancer Res 2001;7:314–9.
3. Denmeade SR, Lin XS, Isaacs JT. Role of programmed (apoptotic) cell death during the progression and therapy for prostate cancer. Prostate 1996;28:251–65.
4. Xu L, Frederik P, Pirollo KF, et al. Self-assembly of a virus-mimicking nanostructure system for efficient tumor-targeted gene delivery. Hum Gene Ther 2002;13:469–81.
5. DiPaola RS, Patel J, Rafi MM. Targeting apoptosis in prostate cancer. Hematol Oncol Clin North Am 2001;15:509–24.
6. Amantana A, London CA, Iversen PL, Devi GR. X-linked inhibitor of apoptosis protein inhibition induces apoptosis and enhances chemotherapy sensitivity in human prostate cancer cells. Mol Cancer Ther 2004;3:699–707.
7. Devi GR. XIAP as target for therapeutic apoptosis in prostate cancer. Drug News Perspect 2004;17:127–34.
8. Salvesen GS, Duckett CS. IAP proteins: blocking the road to death's door. [Review] [154 refs]. Nat Rev Mol Cell Biol 2002;3:401–10.
9. Schimmer AD. Inhibitor of apoptosis proteins: translating basic knowledge into clinical practice. Cancer Res 2004;64:7183–90.
10. Deveraux QL, Takahashi R, Salvesen GS, Reed JC. X-linked IAP is a direct inhibitor of cell-death proteases. Nature 1997;388:300–4.
11. Tenev T, Zachariou A, Wilson R, Ditzel M, Meier P. IAPs are functionally non-equivalent and regulate effector caspases through distinct mechanisms. Nat Cell Biol 2005;7:70–7.
12. Notarbartolo M, Cervello M, Poma P, Dusonchet L, Meli M, D'Alessandro N. Expression of the IAPs in multidrug resistant tumor cells. Oncol Rep 2004;11:133–6.
13. Deveraux QL, Roy N, Stennicke HR, et al. IAPs block apoptotic events induced by caspase-8 and cytochrome *c* by direct inhibition of distinct caspases. EMBO J 1998;17:2215–23.
14. Zhou L, Yuan R, Serggio L. Molecular mechanisms of irradiation-induced apoptosis. Front Biosci 2003;8:d9–19.
15. Du C, Fang M, Li Y, Li L, Wang X. Smac, a mitochondrial protein that promotes cytochrome *c*-dependent caspase activation by eliminating IAP inhibition. Cell 2000;102:33–42.
16. Ohnishi K, Scuric Z, Schiestl RH, Okamoto N, Takahashi A, Ohnishi T. siRNA targeting NBS1 or XIAP increases radiation sensitivity of human cancer cells independent of TP53 status. Radiat Res 2006;166:454–62.
17. Yamaguchi Y, Shiraki K, Fuke H, et al. Targeting of X-linked inhibitor of apoptosis protein or survivin by short interfering RNAs sensitize hepatoma cells to TNF-related apoptosis-inducing ligand- and chemotherapeutic agent-induced cell death. Oncol Rep 2005;14:1311–6.
18. Srinivasula SM, Datta P, Fan XJ, Fernandes-Alnemri T, Huang Z, Alnemri ES. Molecular determinants of the caspase-promoting activity of Smac/DIABLO and its role in the death receptor pathway. J Biol Chem 2000;275:36152–7.
19. Sun H, Nikolovska-Coleska Z, Yang CY, et al. Structure-based design, synthesis, and evaluation of conformationally constrained mimetics of the second mitochondria-derived activator of caspase that target the X-linked inhibitor of apoptosis protein/caspase-9 interaction site. J Med Chem 2004;47:4147–50.
20. Sun H, Nikolovska-Coleska Z, Yang CY, et al. Structure-based design of potent, conformationally constrained Smac mimetics. J Am Chem Soc 2004;126:16686–7.
21. Kalikin LM, Schneider A, Thakur MA, et al. *In vivo* visualization of metastatic prostate cancer and quantitation of disease progression in immunocompromised mice. Cancer Biol Ther 2003;2:656–60.
22. Xu L, Yang D, Wang S, et al. (-)-Gossypol enhances response to radiation therapy and results in tumor regression of human prostate cancer. Mol Cancer Ther 2005;4:197–205.
23. Maine GN, Burstein E. COMMD proteins and the control of the NF κB pathway. Cell Cycle 2007;6:672–6.
24. Srinivasula SM, Hegde R, Saleh A, et al. A conserved XIAP-interaction motif in caspase-9 and Smac/DIABLO regulates caspase activity and apoptosis [comment]. Nature 2001;410:112–6. Erratum in Nature 2001;411:1081.
25. Liu Z, Sun C, Olejniczak ET, et al. Structural basis for binding of Smac/DIABLO to the XIAP BIR3 domain. Nature 2000;408:1004–8.
26. Ahn KS, Sethi G, Aggarwal BB. Embelin, an inhibitor of X chromosome-linked inhibitor-of-apoptosis protein, blocks nuclear factor-κB (NF-κB) signaling pathway leading to suppression of NF-κB-regulated antiapoptotic and metastatic gene products. Mol Pharmacol 2007;71:209–19.

Downloaded from http://aacrjournals.org/clincancerres/article-pdf/14/23/7701/1978518/7701.pdf by guest on 31 January 2023

27. Magne NTR, Bottero V, Didelot C, Houtte PV, Gerard JP, Peyron JF. NF-κB modulation and ionizing radiation: mechanisms and future directions for cancer treatment. Cancer Lett 2006;231:158–68.

28. Voboril R, Weberova-Voborilova J. Constitutive NF-κB activity in colorectal cancer cells: impact on radiation-induced NF-κB activity, radiosensitivity, and apoptosis. Neoplasma 2006;53:518–23.

29. Wang CY, Mayo MW, Korneluk RG, Goeddel DV, Baldwin AS, Jr. NF-κB antiapoptosis: induction of TRAF1 and TRAF2 and c-IAP1 and c-IAP2 to suppress caspase-8 activation. Science 1998;281:1680–3.

30. Nikolovska-Coleska Z, Xu L, Hu Z, et al. Discovery of embelin as a cell-permeable, small-molecular weight inhibitor of XIAP through structure-based computational screening of a traditional herbal medicine three-dimensional structure database. J Med Chem 2004;47:2430–40.

31. Lu M, Lin SC, Huang Y, et al. XIAP induces NF-κB activation via the BIR1/TAB1 interaction and BIR1 dimerization. Mol Cell 2007;26:689–702.

32. Li L, Thomas RM, Suzuki H, De Brabander JK, Wang X, Harran PG. A small molecule Smac mimic potentiates TRAIL- and TNFα-mediated cell death. Science 2004;305:1471–4.

33. Suh J, Rabson AB. NF-κB activation in human prostate cancer: important mediator or epiphenomenon? J Cell Biochem 2004;91:100–17.

34. Jung M, Dritschilo A. NF-κB signaling pathway as a target for human tumor radiosensitization. Semin Radiat Oncol 2001;11:346–51.

35. Brach MA, Hass R, Sherman ML, Gunji H, Weichselbaum R, Kufe D. Ionizing radiation induces expression and binding activity of the nuclear factor κB. J Clin Invest 1991;88:691–5.

36. Varfolomeev E, Blankenship JW, Wayson SM, et al. IAP antagonists induce autoubiquitination of c-IAPs, NF-κB activation, and TNFα-dependent apoptosis. Cell 2007;131:669–81.

37. Vince JE, Wong WW, Khan N, et al. IAP antagonists target cIAP1 to induce TNFα-dependent apoptosis. Cell 2007;131:682–93.

38. Petersen SL, Wang L, Yalcin-Chin A, et al. Autocrine TNFα signaling renders human cancer cells susceptible to Smac-mimetic-induced apoptosis. Cancer Cell 2007;12:445–56.

39. Hindson B, Turner S, Do V. Palliative radiation therapy for localized prostate symptoms in hormone refractory prostate cancer. Australas Radiol 2007;51:584–8.

Downloaded from http://aacrjournals.org/clincancerres/article-pdf/14/23/7701/1978518/7701.pdf by guest on 31 January 2023